ACS APPLIED ELECTRONIC MATERIALS

Article

Cite This: ACS Appl. Electron. Mater. 2019, 1, 2076−2085

pubs.acs.org/acsaelm

Unidirectional Threshold Switching Induced by Cu Migration with High Selectivity and Ultralow OFF Current under Gradual Electroforming Treatment

Putu A. Dananjaya, Desmond J. J. Loy, Samuel C. W. Chow, and Wen Siang Lew*

School of Physical and Mathematical Sciences, Nanyang Technological University, 21 Nanyang Link, Singapore 637371, Singapore

Supporting Information

ABSTRACT: A gradual electroforming process was implemented on the pristine Pt/HfO_x/Cu/Pt structure to realize volatile threshold switching characteristics of a diffusive memristor. The reported devices exhibit stable unidirectional threshold switching properties with high selectivity of $>10^7$ and ultralow OFF current of ∼100 fA for over 10^4 endurance cycles. Nucleation theory on spheroidal-shaped metallic filament growth is used to extensively discuss the structural changes of the device after gradual forming treatments by analyzing the applied bias amplitude dependency of the finite delay time required by the device to turn ON under external electric field. On the other hand, the Rayleigh instability model was implemented for the aforementioned spheroidal metallic nucleus to explain the relaxation dynamics of the device. It was shown that the relaxation time of the device depends on the initial profile of the nucleus within the insulating layer. The broadening of the ON current distribution of the device was observed during the device endurance test. This is correlated to the presence of a random telegraph signal (RTS) during the ON state of the device.

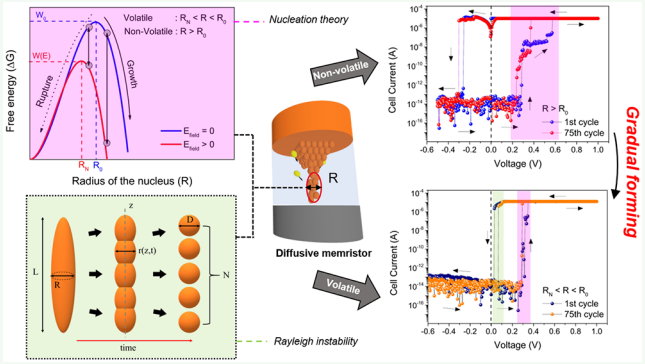

KEYWORDS: *threshold switching, diffusive memristor, nucleation theory, Rayleigh instability, random telegraph signal*

INTRODUCTION

Memristive devices are promising nonvolatile memory technologies due to its high scalability, high-speed operation, low power consumption, and multibit per cell capability. These desirable characteristics are required for both embedded and stand-alone mass storage devices. Recently, the artificial intelligence technology, which utilizes a new high-level computing approach, has been on a quest in search of ideal synaptic devices to realize a highly dense computing platform, which requires high synaptic weight precision. Thus, the high scalability nature and multibit per cell capability demonstrated in many memristive devices have attracted a great deal of attention from the neuromorphic computing community to fulfill their ideal synaptic device requirements.

To fully utilize the scalability of a memristive device through highly connected crossbar array, a select device or selector is required to work in tandem with the memory element to mitigate the inherent sneak path current issue of the architecture. In the recent years, different types of selectors have been widely investigated. These selectors can be classified into two major categories, i.e., nonlinear IV and threshold IV selector. Nonlinear IV selectors are those devices utilizing metal oxide Schottky barrier modulation,[1−7] crested and variable oxide tunnel barrier,[8−13] and mixed ionic electronic conduction (MIEC).[14−17] On the other hand, the threshold IV selector consists of ovonic threshold switches (OTSs),[18−20] metal−insulator transition (MIT) devices,[21−24] and diffusive memristors (DMs).[7,25−45] Among these select devices, DM has been found to exhibit the most promising performance in terms of selectivity and OFF current. In addition to the crossbar array integration, DM devices, due to their distinctive device dynamics, are implemented in emerging systems, e.g., true random number generators,[27] steep subthreshold slope transistors,[30,33] and artificial synaptic devices.[28,29,37]

The reported DM devices can be classified as Ag[7,25−40] and Cu[40−45] based devices. DM devices work based on the electric-field-induced migration of active metal atoms, e.g., Cu and Ag, with high mobility inside the dielectric layer. The device is switched ON when the applied electric field exceeds the threshold field required to form unstable metallic filament within the dielectric and is switched OFF due to its dissolution after the removal of the electric field. This mechanism is analogous to electrochemical metallization (ECM) cells. The same structure might exhibit both nonvolatile and volatile switching characteristics, which can be used for memory and threshold switch applications, respectively.[35,44] Thus, complete

Received: July 16, 2019
Accepted: September 26, 2019
Published: October 9, 2019

DOI: 10.1021/acsaelm.9b00446
ACS Appl. Electron. Mater. 2019, 1, 2076−2085

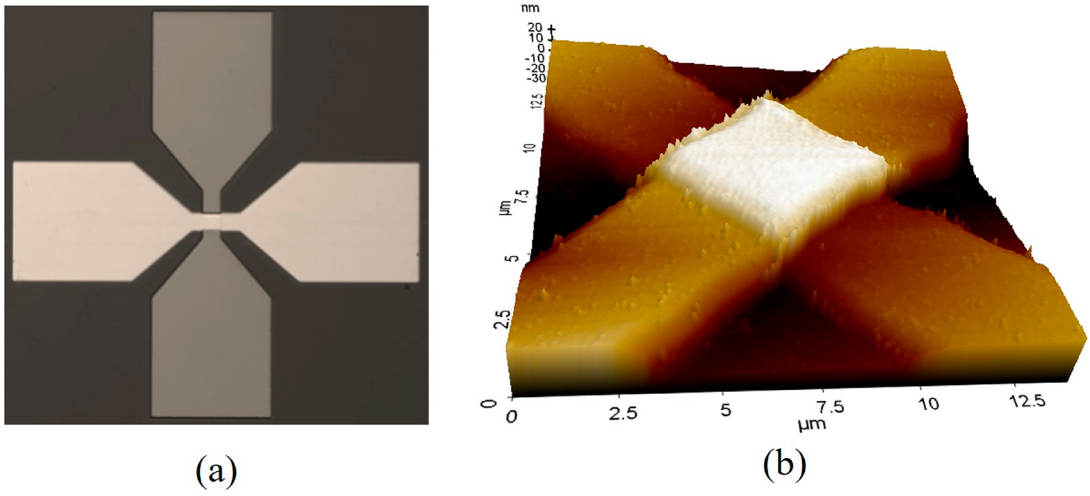

Figure 1. (a) Top view of the crosspoint device under an optical microscope. (b) 3D view of the structure taken by atomic force microscopy.

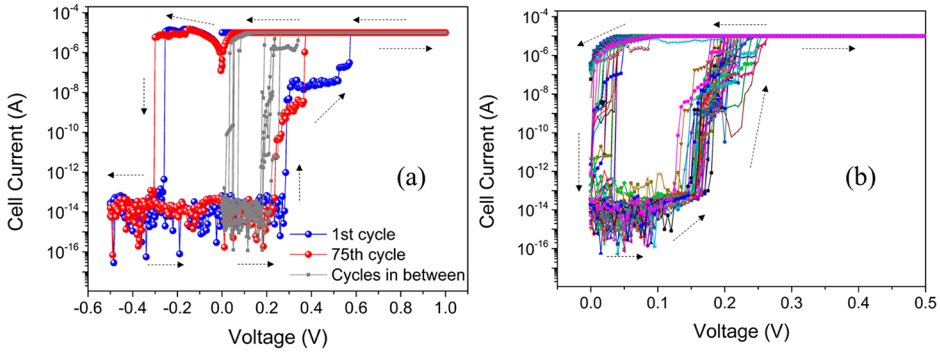

Figure 2. Behavior of the devices underwent direct electroforming under 10 μA CC showed a mix of volatile and nonvolatile switching behavior in between cycles (a), while the devices underwent gradual forming treatment exhibited pure volatile threshold switching characteristics (b).

control over these two opposite characteristics must be thoroughly investigated.

In this work, a gradual electroforming process from pristine Pt/HfO_x/Cu/Pt structure is introduced to achieve volatile threshold switching rather than nonvolatile memory characteristics. Crosspoint device structures of 10 μm × 10 μm cell area, shown in Figure 1, were fabricated by a two-step UV-lithography patterning followed by lift-off process. All materials in the structure were deposited via magnetron sputtering deposition, i.e., DC sputtering for metals and RF sputtering from ceramic target (HfO_2) for the oxide layer. The thickness of each layer in the structure is 10 nm. The electrical characterizations were done using a Keithley 4200A-SCS parameter analyzer, i.e., source measure unit (SMU) and preamplifier for DC IV measurement and pulse measure unit (PMU) for fast IV measurement.

GRADUAL FORMING PROCESS AND THRESHOLD SWITCHING CHARACTERISTICS OF DM

To specifically achieve threshold switching properties, two common fabrication techniques have been implemented. The first technique involves cosputtering and/or reactive sputtering deposition to form metal (Cu or Ag) and insulating host composites. It requires high control over the number of metal atoms within the insulating host. The second technique utilizes a postannealing treatment to allow metal atoms diffusion into insulating layer. Temperature and duration of the annealing process are the two critical parameters to achieve the desired properties. Because of the bulk nature of the atomic diffusion, it usually requires an insertion of a thin tunneling layer to maintain the high selectivity of the threshold switch. HfO_x/Cu-based structures have been reported as to exhibit both memristive and threshold switching properties within one structure. This technique was implemented to alter the memristive property of the device into volatile threshold switching characteristics.[44] However, the temporal response of the device has not been discussed.

It has been reported that the compliance current (CC) during the operation of DM plays an important role in controlling the nature of metallic filament induced under external electric field.[26,35,45] Relatively higher CCs have been observed to result in nonvolatile memory switching behavior, while the lower CCs lead to unstable metallic filament resulting in volatile threshold switching characteristics. For the structure investigated in this work, the ON state current target was set to be 10 μA or higher, which was based on the common switching current range reported for memristive devices. The devices underwent direct forming by using a compliance current of 10 uA or higher tend to form a strong conductive filament, which resulted in nonvolatile switching behavior, depicted in Figure 2

The electroforming process was performed by gradually increasing the CC from 100 nA to 10 μA with a certain subsequent CC ratio. Two critical parameters in the gradual forming treatment are the starting CC value and the

DOI: 10.1021/acsaelm.9b00446
ACS Appl. Electron. Mater. 2019, 1, 2076−2085

subsequent CC ratio. It was found that the optimized forming condition to achieve stable volatile threshold switching characteristics was with the starting CC of 100 nA and subsequent CC ratio from 2 to 40. More detailed discussion on the implementation of the gradual forming treatment can be found in the Supporting Information.

During the gradual forming treatment, the devices had to undergo long duration of voltage stress under DC sweep. Any structural changes exhibited by the device during this forming process is critical for the subsequent device operation. Thus, a single run and multiple runs (50 cycles) of DC gradual forming treatment for each CC value were conducted to investigate the device structural changes during the forming process.

The gradual forming process allows more controllable and localized metallic filament of ionizable Cu electrode into HfO_x dielectric, shown in Figure 3. A decreasing trend in the

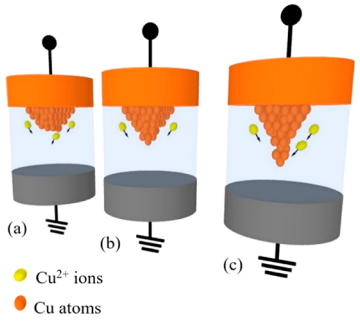

Figure 3. Gradual forming process of the device from the lowest compliance current (a) to the highest one (c).

threshold voltage (V_{th}) of the device was observed with increasing CC value under DC IV sweep, as shown in Figure 4a,b. This is potentially attributed to the amount of Cu atoms residing within dielectric and the effective thickness of the oxide involve during the switching process, which is discussed further in the following segment of the work. After the gradual forming treatment was performed, the device under test was connected to series resistor of 47 kΩ to facilitate subsequent DC cycling and pulse measurements. The forming process was able to successfully achieve stable threshold switching behavior with more than 100 DC cycles (a few selected cycles are shown in Figure 5).

The devices tested also preserved unidirectional characteristics after forming and the subsequent cycles. The

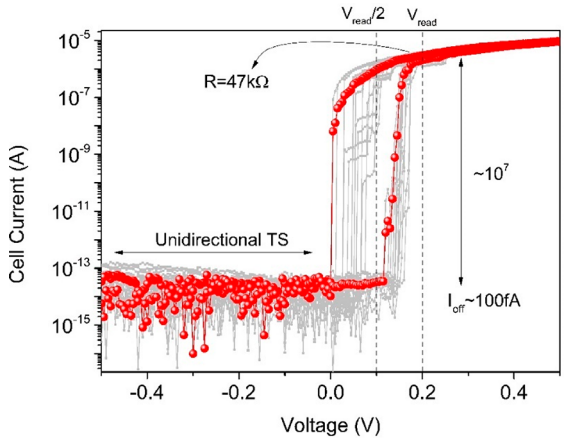

Figure 5. DC IV sweep with series resistor of 47 kΩ connected to the DM device shows the unidirectionality of the DM devices. Ultralow OFF state current about 100 fA and high selectivity of 10^7 was observed under the $V/2$ operating scheme.

unidirectionality of the switching is due to the asymmetrical structure of the devices and the nature of the Cu filament growth within the HfO_x. There are two possible growth mechanisms in Cu-based devices, i.e., filamentary growth of Cu atoms from the active copper electrode toward the inert electrode[46] and filamentary growth in opposite direction.[47] This suggests the localized filamentary growth of Cu atoms from the active copper electrode toward the inert electrode[46] rather than the localized filamentary growth in the opposite direction during gradual forming of the device.[47] Asymmetrical structures exhibiting bidirectional volatile switching behavior have only been reported in Ag-based devices.[25,48,49] This is consistent with reported literatures on the observation of Ag filament growth.[35,50] The Ag conductive filaments tend to grow from the inert electrode toward the active electrode. Thus, when the unstable filament formed during volatile switching process, the rupture of the filament does not occur at the furthest Ag atoms position from active electrode, which will leave Ag atoms residue on the inert electrode. After the first few switching cycles of the Ag-based DM devices, there will be a sufficient amount of Ag atoms on both side of the dielectric to achieve bidirectional volatile threshold switching behavior. This asymmetrical structure will not be able to achieve bidirectional selector behavior in as-fabricated devices.

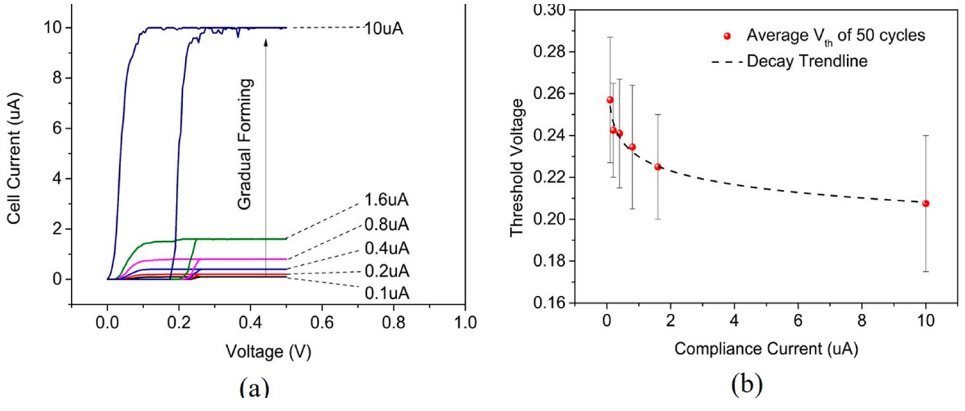

Figure 4. (a) DC IV sweep of gradual forming treatment. (b) Decreasing trend of threshold voltage with the increase of compliance current.

DOI: 10.1021/acsaelm.9b00446
ACS Appl. Electron. Mater. 2019, 1, 2076−2085

TEMPORAL RESPONSE OF DM DEVICES

The underlying mechanism of DM utilizes the ionic movement of the active electrode inside the dielectric. While it results in an ultralow OFF current and high selectivity, it also leads to the device having a finite delay and relaxation time during ON and OFF operations, respectively. The reported values for delay time vary from about 70 ns up to 70 ms, while the relaxation time varies from 70 ns to 25 s.[48] This temporal response of the device is determined by the specific structure used, applied electric field, and device operating temperature. The focus of this study is on the influence of applied electric field amplitude on the temporal response of the devices.

The time domain measurements were performed by sending higher amplitude voltage pulse to turn ON the DM followed by a "read" pulse of 0.1 V with 20 ms pulse width after a 1 μs interval, while the current flowing through the device was simultaneously measured. Figure 6b shows a complete ON−OFF cycle of the device. The delay time of the device was captured through the time domain measurement from the moment "write" pulse implemented until the observation of abrupt increase in cell current, as depicted in Figure 6a. On the other hand, the finite relaxation time was measured from the timestamp of the removal of the electric field until the sudden drop in cell current was observed, as shown in Figure 6c.

Different pulse amplitudes were implemented from 0.3 to 1.0 V with 10 ms duration to measure the device delay time dependence on external electric field. The delay time decreases exponentially with an increase in external bias amplitude for the different devices under two different forming treatments. This correlation is supported by the field-induced nucleation theory, depicted in Figure 7.[7,51−53] Based on this theory, the metallic filament within the dielectric under an external electric field is caused by the growth of spheroidal metallic nucleus from ionic movements of active electrode atoms inside the dielectric. Stable spheroidal metallic nucleus can only be established if the nucleation energy barrier, $U_N(E)$, is overcome to allow the nucleus growth beyond the critical radius, R_N. This energy barrier is reduced with the presence of external electric field and will return to its equilibrium value, U_0, after the removal of the field. It has been reported that the nucleation leads to volatile switching characteristics if the effective radius of the stable nucleus is lower than R_0, while resulting in nonvolatile switching behavior if it increases past R_0. The delay time of the device can be correlated to the nucleation energy barrier height by the following equation:[7]

$$\tau_d = \tau_0 \exp\left[\frac{U_N(E)}{kT}\right] \quad (1)$$

The temperature of the devices was kept constant at room temperature throughout the experiment. τ_0 is defined as the characteristic delay time, which is unique to the active material and dielectric used in the system. $U_N(E)$ is defined as nucleation energy barrier height, which can be expressed by the following:

$$U_N(E) = U_0 E_0 \alpha^{3/2} \frac{d}{V} \quad (2)$$

V and d are defined as external voltage applied and effective thickness of the dielectric involved during the volatile switching operation. The effective thickness refers to smallest distance between the Cu atoms to the Pt inert electrode across the dielectric. U_0 is defined as the nucleation barrier energy at zero field, which is unique to the dielectric material in which the metal atoms move within, e.g., HfO_x (0.47 eV) and TiO_x (0.71 eV).[7] In this work, the dielectric material used was the same, i.e., HfO_x. Thus, under the two forming treatments, the value of parameter U_0 did not change. E_0 is defined in the literatures as voltage acceleration factor or characteristic field. This value is independent of the external field or temperature. The acceptable value used in calculation is 1 MV/cm,[7] regardless of the type of structures or systems. α is geometric factor of spheroid nucleus. Its value ranges from 0.1 to 0.5, and it was assumed to be 0.5 in the literature because it corresponds to the highest nucleation barrier energy. This value is dependent on the shape of the nucleus. Across

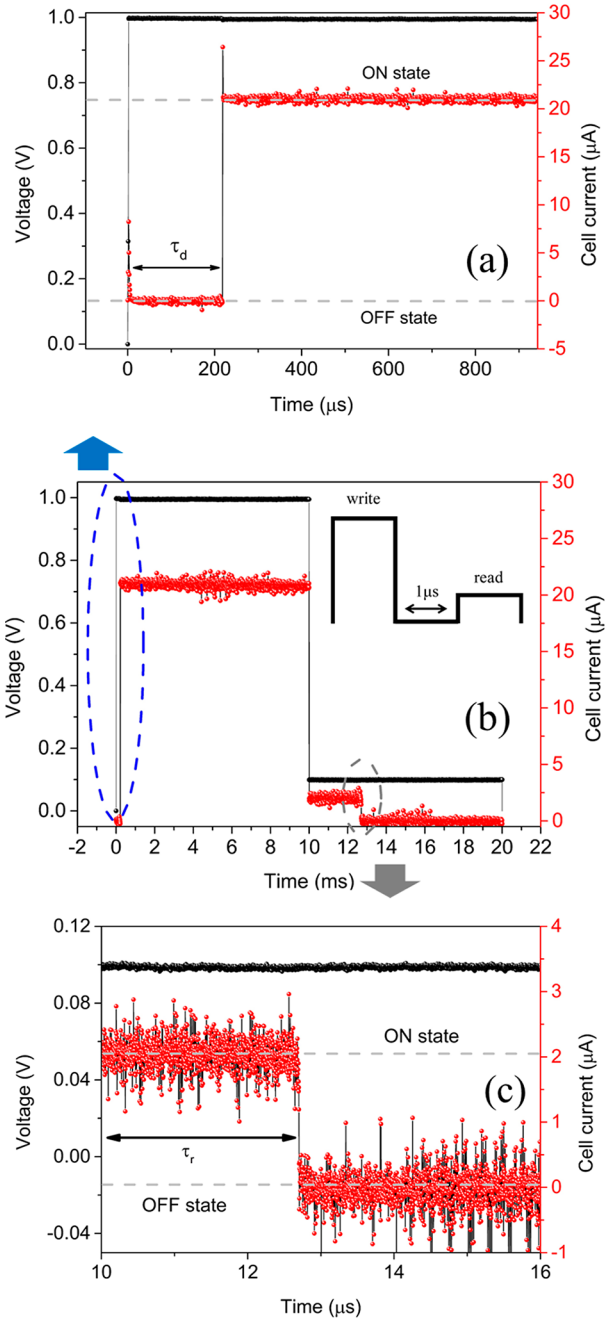

Figure 6. Complete ON−OFF cycle of the time domain measurement of the device (b) to capture device delay time (a) and device relaxation time (c).

DOI: 10.1021/acsaelm.9b00446
ACS Appl. Electron. Mater. 2019, 1, 2076−2085

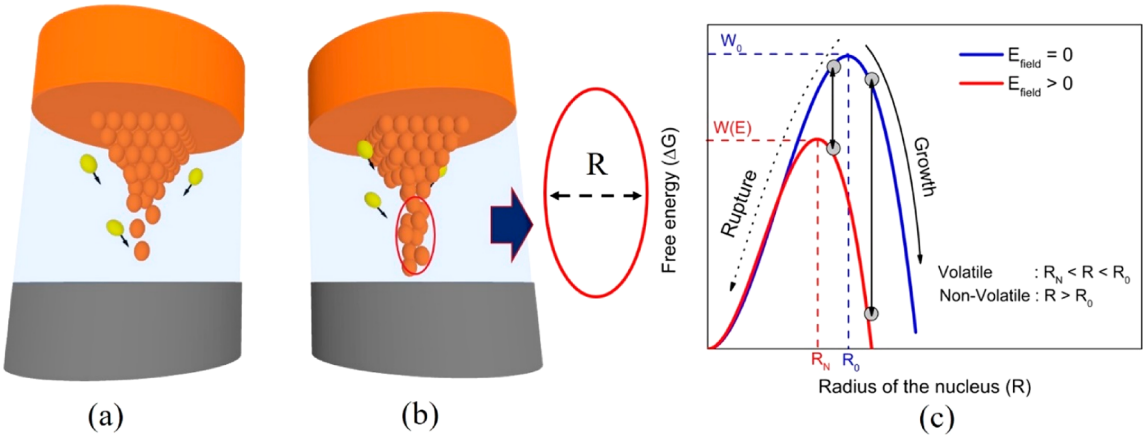

Figure 7. Parts a and b show the schematic of the Cu species arrangement within the HfO_x layer during the OFF and ON state, respectively. Part c illustrates the criteria of achieving volatile and nonvolatile switching characteristics based on field-induced nucleation theory.

different dielectric materials, this value might be different, but within the same dielectric material, this geometric factor can be safely assumed to be identical.

The focus of this segment of the work is to investigate the effect of external electric field (voltage) on the temporal response of the device. Hence, to simplify the expression in (1), another critical parameter ζ is defined to replace $U_N(E)$.

$$\zeta = U_0 E_0 \alpha^{3/2} \frac{d}{kT} \tag{3}$$

Thus, eq 1 can be modified into the following:

$$\tau_d = \tau_0 \exp\left[\frac{\zeta}{V}\right] \tag{4}$$

Equation 4 was used to fit the experimental data obtained for device delay time under different pulse amplitude, shown in Figure 8. The experimental data fit well under field-induced

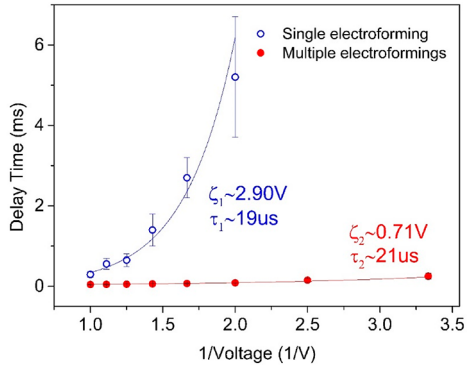

Figure 8. Voltage amplitude dependence of device delay time under single and multiple forming treatments. The extracted characteristic time, τ, values are very close in value which indicates both relations come from the same structure of $Pt/HfO_x/Cu/Pt$.

nucleation theory with a spheroidal-shaped metallic filament. The device delay time varies from ~5 ms to under 300 μs for the single run forming treatment, while it ranges from 250 μs to as fast as 44 μs for multiple runs forming treatment under different voltage amplitudes. Two parameters could be extracted from the fitting curves, i.e., τ_0 and ζ. τ_0 values extracted from the fitting are ~19 and ~21 μs for devices that underwent single and multiple forming treatments, respectively. This is consistent in which the two forming conditions are strictly comparing the same $Pt/HfO_x/Cu/Pt$ structures. On the other hand, the extracted ζ values under two different forming treatments exhibit a significant difference. Based on the field nucleation theory, it is attributed to the change in the effective thickness of the oxide layer involved throughout the nucleation process. It was found that the value of ζ_1 is about 4 times higher than ζ_2. The devices that underwent single forming treatment were assumed to have a very small change in the effective thickness from the pristine devices, i.e., $d \sim 10$ nm. The thickness of the HfO_x layer in the pristine devices was experimentally confirmed by TEM images of the multilayer structure, as shown in Figure S3. This indicates the effective thickness of the oxide was reduced significantly from ~10 nm originally to ~2.5 nm.

The relaxation time of the device was also investigated under different voltage amplitudes in the range 0.8−1.2 V with 10 ms pulse width. From Figure 9, an increasing trend of relaxation

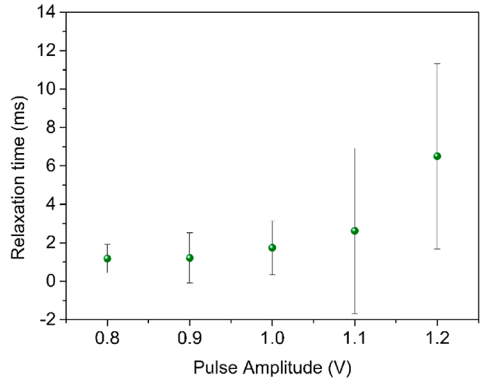

Figure 9. Increasing trend of average relaxation time of the device observed under increasing voltage pulse amplitude.

time was observed from about 1 to 7 ms with an increase of voltage amplitudes. This trend is potentially due to the size of the spheroidal nucleus generated under different voltage pulses. The higher the amplitude of the pulse, the stronger or larger metallic nucleus dimension formed. Thus, a larger metallic nucleus will take a relatively longer time to rupture after the removal of the electric field.

This observation is supported by the Rayleigh instability model of the metallic filament rupture inside the dielec-

DOI: 10.1021/acsaelm.9b00446
ACS Appl. Electron. Mater. 2019, 1, 2076−2085

tric.[26,36,37,40] Rayleigh instability suggests that after a removal of an electric field the metallic filament ruptures into a series of spherical nanoclusters through the minimization of total free energy of the system. With our earlier confirmation on spheroidal metallic nucleus growth by looking at the device delay time dependency on voltage pulse amplitude, the initial filament shape before the removal of electric field is taken as a spheroid, as shown in Figure 10. Thus, an analytical model was

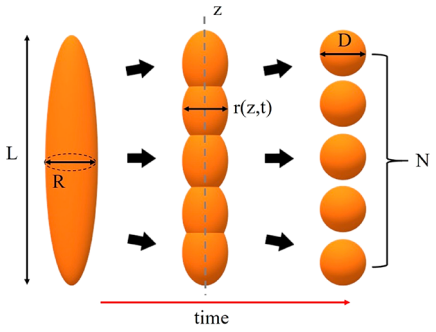

Figure 10. Metallic filament dissolution process based on the Rayleigh instability theorem.

proposed to better understand the evolution of filament morphology. After the removal of the electric field, the spheroidal nucleus is divided into N number of nanospheres. This process is assumed to be due to the atomistic rearrangement of Cu atoms, causing the total volume of the shape to be constant throughout the process. The number of Cu spherical nanoclusters (N) formed can be expressed as

$$N = \rho\frac{R^3}{D^3} \tag{5}$$

where ρ is defined as aspect ratio of L/R, in which L and R are the initial major and minor axis dimension of the nucleus, respectively. D is defined as the average diameter of nanoclusters formed in the OFF state of the device. This phase transition is driven by the change in total free energy consists of both surface and volume terms. However, with the assumption of constant volume throughout the process, the change in surface free energy will be the only terms contributing into the system. By approximation of very thin metallic filament ($\rho \gg 1$), the change in free energy was estimated by the following equation:

$$\Delta G \approx \pi\rho R^2\left(\frac{R}{D} - \frac{\pi}{4}\right) \tag{6}$$

Spontaneous evolution of the filament after the removal of the electric field has been experimentally confirmed in the rupture of Ag filament as per this literature.[26] Thus, the change in free energy should be less than zero, and the dimension of the nanoclusters should follow the relation

$$D > \frac{4}{\pi}R \tag{7}$$

After longitudinal damped sinusoidal perturbation is applied along the major axis of the spheroid, the surface perturbation equation is given by

$$r(z, t) = R(z) + \delta_2(t)\delta_1(z)\sin kz \tag{8}$$

where k is the perturbation wavenumber along the z-axis and $\delta_1(z)$ and $\delta_2(t)$ are the spatial and temporal dependence of the perturbation amplitude terms, respectively. While the temporal dependence of the perturbation amplitude has been frequently reported,[26,36,37,40] the spatial dependence of the amplitude was added due to the spheroidal nature of the filament. If $z = z_N$ was taken as the center point of one of the nanospheres, the relaxation time of the device is determined by the following equation:

$$\delta_2(\tau_d) = \frac{D - R(z_N)}{\delta_1(z_N)\sin kz_N} \tag{9}$$

From this equation, it was concluded that the relaxation time is mainly driven by initial filament profile, which is driven by the current or voltage amplitude during the "write" operation.

RELIABILITY ASPECTS OF DM: DEVICE ENDURANCE AND OBSERVATION OF RANDOM TELEGRAPH SIGNAL (RTS)

The endurance test was performed on a device that underwent multiple runs of forming treatment. By using the correlation of pulse amplitude to the delay time of the device in Figure 8, the endurance test was performed by sending 200 μs of 0.4 V pulse to turn ON the device and 200 μs of 0.2 V pulse to measure the OFF state of the device. The OFF state of the device was beyond the measurement limit of the equipment. No selectivity degradation was observed after more than 10^4 cycles, shown in Figure 11. The current distribution of the ON state was observed to be lower than the current flow of 1-

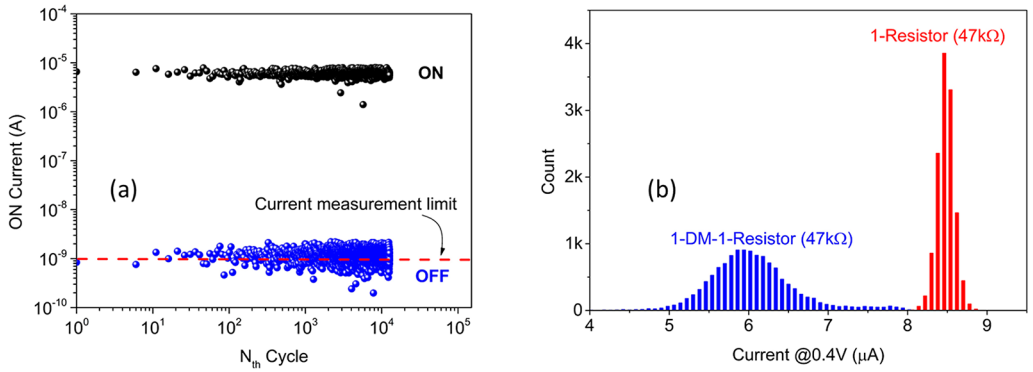

Figure 11. (a) Actual endurance cycle reading of the device with over 10^4 ON−OFF cycles. (b) Comparison of current distribution between 1-DM-1Resistor and 1-Resistor under 0.4 V voltage amplitude.

DOI: 10.1021/acsaelm.9b00446
ACS Appl. Electron. Mater. 2019, 1, 2076−2085

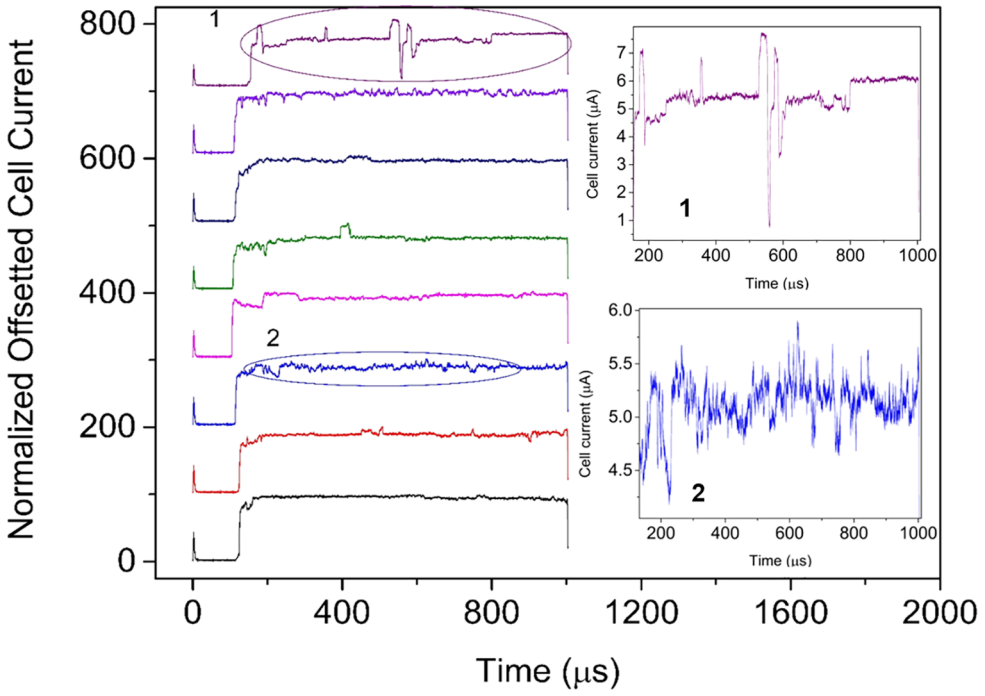

Figure 12. RTS captured from different cycles operation of the device during the ON state under 0.4 V voltage amplitude. Unstable complex RTS was observed exhibiting multilevel RTS nature.

Resistor under the same voltage, which means the DM device reached a comparable resistance value to that of the resistor as expected. However, the distribution of the current of DM device was noticeably asymmetrical and has broader variation compared to 1-Resistor current.

The origin of the ON-state current variation is explained by the presence of random telegraph signal (RTS) in DM devices. RTS is defined a as random bimodal or multilevel fluctuation of current or voltage during device operation. RTS has been widely reported in memristive devices, especially oxide-based devices utilizing the movement of oxygen ions and/or oxygen vacancy-type defects modification for its operations. For these types of devices, the origin of the RTS is believed to be from the reversible movement of electrons between metal electrodes and defects within dielectric layer which is also known as charge trapping and detrapping activities.[54] However, the DM device structure and underlying switching mechanism mimic those of electrochemical metallization cells (ECM). Thus, the origin of RTS in DM devices is expected to incline toward those similar types of devices in which very few studies have been conducted. In Cu-doped $Ge_{0.3}Se_{0.7}$ devices, it is suggested that the RTS presence in the device is potentially due to thermally activated movement of Cu species within ionic or redox "double-site traps".[55] Another report on Ge_xSe_{1-x}-based devices showed the observation of RTS in ovonic threshold switching mechanism after the forming process.[56] Figure 12 shows different RTS observed in the DM structure during the ON state of the device under 0.4 V voltage amplitude. Both bimodal and multilevel RTS were observed within the same structure but under different writing cycles. This demonstrated the random and complex nature of the signal. The current readings of the device ON and OFF states during the endurance test were done by taking the average of the data points at the same 10 μs window. Thus, with the time domain variation of RTS, the cell current distribution would be larger than the current distribution of the 1-R configuration.

Further investigation of the RTS behavior was performed under different applied voltage amplitudes. Two different types of RTS were observed in different voltage regimes, depicted in Figure 13. The first RTS was more dominantly observed in the low-voltage regime ($\leq$0.6 V), resulting in random fluctuations throughout the ON state of the device. It was the same type of RTS causing the current distribution broadening during endurance test at 0.4 V. This RTS became less apparent with the increase of the external applied voltage. The second RTS was observed in the high voltage regime of more than 0.6 V. This RTS was more likely to be observed in the early stage of the ON state rather than throughout the ON state. This could be attributed to the competing nature of the two parameters, i.e., external electric field and Joule heating. A higher electric field tends to result in a stronger filament, but at the same time it will generate a larger Joule heating effect that might rupture the metal filament. The current reading was observed to stabilize after several current jumps. This could be an indication of a stronger and larger filament had been formed after several ruptures. This property must be taken into consideration in the device implementation as a select device in crossbar array, especially during the "write" operation of the memory cell that requires a higher voltage amplitude. The average time constant of this behavior was above 10 μs. Thus, it will not affect the memory operation of the devices operating in the faster regime in which most of the reported memristive devices stand.

CONCLUSIONS

This work has provided a new technique, from a device operation point of view, to achieve volatile threshold switching behavior from the pristine Pt/HfO_x/Cu/Pt structure via gradual electroforming treatment. Excellent selectivity of more than 10^7 and extremely low OFF current of 100 fA were maintained with more than 10^4 ON−OFF cycles. An insight into the structural evolution of the DM was discussed

DOI: 10.1021/acsaelm.9b00446
ACS Appl. Electron. Mater. 2019, 1, 2076−2085

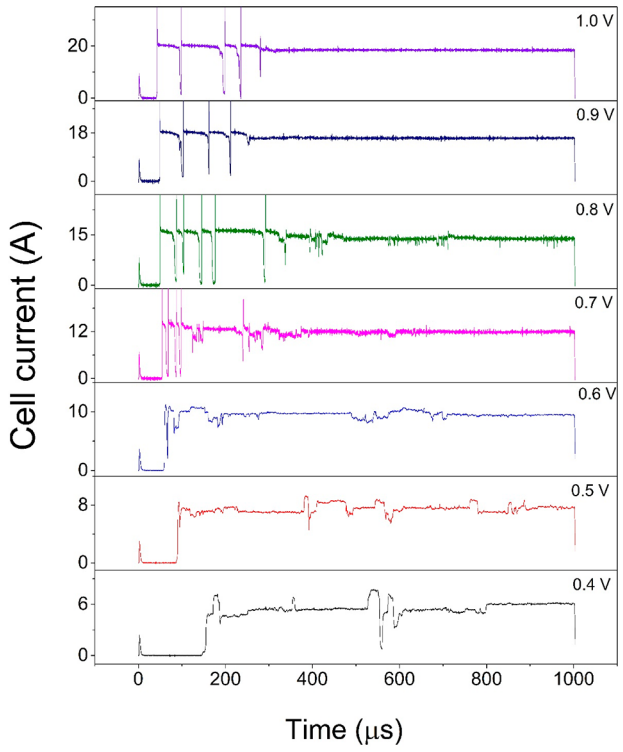

Figure 13. RTS behavior was observed under different voltage amplitudes. Red-dashed lines are the current peak due to measurement settling time, and the black-dashed line indicates the current flow of the 1-R configuration (taking a current reading of 1.0 V as an example).

by analyzing the temporal response of the device under different external electric fields in the frame of the field-induced nucleation theory and Rayleigh instability model. This analysis can be potentially used to extrapolate the device degradation mechanism in which excessive amount of copper species eventually reside within the insulating layer. The reliability aspect of the device considering the current distribution broadening observed during endurance test was also discussed. It was caused by the presence of RTS originating from thermally induced Cu ionic or redox "double-site trap" activities in the structure. The RTS dependence on external applied voltages was also investigated, which gives an important insight into the time domain behavior of the device under different voltage regimes.

■ ASSOCIATED CONTENT

Supporting Information

The Supporting Information is available free of charge on the ACS Publications website at DOI: 10.1021/acsaelm.9b00446.

Volatile threshold switching characteristics achieved under 100 nA and 1 μA without gradual forming treatment (Figure S1); characteristics of the devices under gradual forming treatment with starting CC of 100 nA and subsequent CC ratio of 2 and 40 (Figure S2); behavior of the devices under starting CC of 100 nA and subsequent CC ratio of 40 (Figure S3); cross-sectional TEM image of the pristine 10 × 10 μm^2 device (Figure S4) (PDF)

■ AUTHOR INFORMATION

Corresponding Author

*E-mail wensiang@ntu.edu.sg.

ORCID

Putu A. Dananjaya: 0000-0001-9416-6455

Wen Siang Lew: 0000-0002-5161-741X

Author Contributions

P.A.D. and S.C.W. fabricated the devices. P.A.D. conducted the measurements. P.A.D., D.J.J.L., S.C.W.C., and W.S.L. wrote the manuscript. All authors have approved the final version of the manuscript.

Notes

The authors declare no competing financial interest.

■ ACKNOWLEDGMENTS

This work was supported by a RIE2020 ASTAR AME IAF-ICP Grant (No. I1801E0030) and an ASTAR AME Programmatic Grant (No. A1687b0033). W.S.L. is also a member of the SG-SPIN Consortium.

■ REFERENCES

(1) Huang, J.; Tseng, Y.; Hsu, C.; Hou, T. Bipolar Nonlinear Ni/TiO_2/Ni Selector for 1S1R Crossbar Array Applications. *IEEE Electron Device Lett.* **2011**, *32* (10), 1427−1429.

(2) Huang, J.; Yi-Ming, T.; Wun-Cheng, L.; Chung-Wei, H.; Hou, T. In *One Selector-One Resistor (1S1R) Crossbar Array For High-Density Flexible Memory Applications*; 2011 International Electron Devices Meeting, 5−7 Dec 2011; 2011; pp 31.7.1−31.7.4.

(3) Huang, J.-J.; Kuo, C.-W.; Chang, W.-C.; Hou, T.-H. Transition of Stable Rectification to Resistive-Switching in Ti/Tio_2/Pt Oxide Diode. *Appl. Phys. Lett.* **2010**, *96* (26), 262901.

(4) Kim, G. H.; Lee, J. H.; Han, J. H.; Song, S. J.; Seok, J. Y.; Yoon, J. H.; Yoon, K. J.; Lee, M. H.; Park, T. J.; Hwang, C. S. Schottky Diode with Excellent Performance for Large Integration Density of Crossbar Resistive Memory. *Appl. Phys. Lett.* **2012**, *100* (21), 213508.

(5) Park, W. Y.; Kim, G. H.; Seok, J. Y.; Kim, K. M.; Song, S. J.; Lee, M. H.; Hwang, C. S. A Pt/Tio_2/Ti Schottky-Type Selection Diode for Alleviating The Sneak Current in Resistance Switching Memory Arrays. *Nanotechnology* **2010**, *21* (19), 195201.

(6) Tallarida, G.; Huby, N.; Kutrzeba-Kotowska, B.; Spiga, S.; Arcari, M.; Csaba, G.; Lugli, P.; Redaelli, A.; Bez, R. In *Low Temperature Rectifying Junctions for Crossbar Non-Volatile Memory Devices*; 2009 IEEE International Memory Workshop, 10−14 May 2009; 2009; pp 1−3.

(7) Yoo, J.; Park, J.; Song, J.; Lim, S.; Hwang, H. Field-Induced Nucleation in Threshold Switching Characteristics of Electrochemical Metallization Devices. *Appl. Phys. Lett.* **2017**, *111* (6), 063109.

(8) Kawahara, A.; Azuma, R.; Ikeda, Y.; Kawai, K.; Katoh, Y.; Hayakawa, Y.; Tsuji, K.; Yoneda, S.; Himeno, A.; Shimakawa, K.; Takagi, T.; Mikawa, T.; Aono, K. An 8 Mb Multi-Layered Cross-Point ReRAM Macro with 443 MB/s Write Throughput. *IEEE J. Solid-State Circuits* **2013**, *48* (1), 178−185.

(9) Lee, W.; Park, J.; Kim, S.; Woo, J.; Shin, J.; Choi, G.; Park, S.; Lee, D.; Cha, E.; Lee, B. H.; Hwang, H. High Current Density and Nonlinearity Combination of Selection Device Based on TaO_x/TiO_2/TaO_x Structure for One Selector−One Resistor Arrays. *ACS Nano* **2012**, *6* (9), 8166−8172.

(10) Lee, W.; Park, J.; Shin, J.; Woo, J.; Kim, S.; Choi, G.; Jung, S.; Park, S.; Lee, D.; Cha, E.; Lee, H. D.; Kim, S. G.; Chung, S.; Hwang, H. In *Varistor-Type Bidirectional Switch (J_{max} > 10^7 A/Cm^2, Selectivity ~ 10^4) for 3D Bipolar Resistive Memory Arrays*; 2012 Symposium on VLSI Technology (VLSIT), 12−14 June 2012; 2012; pp 37−38.

(11) Shin, J.; Kim, I.; Biju, K. P.; Jo, M.; Park, J.; Lee, J.; Jung, S.; Lee, W.; Kim, S.; Park, S.; Hwang, H. Tio_2-Based Metal-Insulator-Metal Selection Device for Bipolar Resistive Random Access Memory Cross-Point Application. *J. Appl. Phys.* **2011**, *109* (3), 033712.

DOI: 10.1021/acsaelm.9b00446
ACS Appl. Electron. Mater. 2019, 1, 2076−2085

(12) Woo, J.; Lee, D.; Cha, E.; Lee, S.; Park, S.; Hwang, H. Multilayer-Oxide-Based Bidirectional Cell Selector Device for Cross-Point Resistive Memory Applications. *Appl. Phys. Lett.* **2013**, *103* (20), 202113.
(13) Woo, J.; Lee, W.; Park, S.; Kim, S.; Lee, D.; Choi, G.; Cha, E.; Lee, J. h.; Jung, W. Y.; Park, C. G.; Hwang, H. In *Multi-Layer Tunnel Barrier ($Ta_2O_5/TaO_x/TiO_2$) Engineering for Bipolar RRAM Selector Applications*; 2013 Symposium on VLSI Technology, 11−13 June 2013; 2013; pp T168−T169.
(14) Burr, G. W.; Virwani, K.; Shenoy, R. S.; Padilla, A.; BrightSky, M.; Joseph, E. A.; Lofaro, M.; Kellock, A. J.; King, R. S.; Nguyen, K.; Bowers, A. N.; Jurich, M.; Rettner, C. T.; Jackson, B.; Bethune, D. S.; Shelby, R. M.; Topuria, T.; Arellano, N.; Rice, P. M.; Kurdi, B. N.; Gopalakrishnan, K. In *Large-Scale (512kbit) Integration of Multilayer-Ready Access-Devices Based on Mixed-Ionic-Electronic-Conduction (Miec) at 100% Yield*; 2012 Symposium on VLSI Technology (VLSIT), 12−14 June 2012; 2012; pp 41−42.
(15) Gopalakrishnan, K.; Shenoy, R. S.; Rettner, C. T.; Virwani, K.; Bethune, D. S.; Shelby, R. M.; Burr, G. W.; Kellock, A.; King, R. S.; Nguyen, K.; Bowers, A. N.; Jurich, M.; Jackson, B.; Friz, A. M.; Topuria, T.; Rice, P. M.; Kurdi, B. N. In *Highly-Scalable Novel Access Device Based on Mixed Ionic Electronic Conduction (Miec) Materials for High Density Phase Change Memory (PCM) Arrays*; 2010 Symposium on VLSI Technology, 15−17 June 2010; 2010; pp 205−206.
(16) Shenoy, R. S.; Gopalakrishnan, K.; Jackson, B.; Virwani, K.; Burr, G. W.; Rettner, C. T.; Padilla, A.; Bethune, D. S.; Shelby, R. M.; Kellock, A. J.; Breitwisch, M.; Joseph, E. A.; Dasaka, R.; King, R. S.; Nguyen, K.; Bowers, A. N.; Jurich, M.; Friz, A. M.; Topuria, T.; Rice, P. M.; Kurdi, B. N. In *Endurance and Scaling Trends of Novel Access-Devices for Multi-Layer Crosspoint-Memory Based on Mixed-Ionic-Electronic-Conduction (Miec) Materials*; 2011 Symposium on VLSI Technology - Digest of Technical Papers, 14−16 June 2011; 2011; pp 94−95.
(17) Virwani, K.; Burr, G. W.; Shenoy, R. S.; Rettner, C. T.; Padilla, A.; Topuria, T.; Rice, P. M.; Ho, G.; King, R. S.; Nguyen, K.; Bowers, A. N.; Jurich, M.; BrightSky, M.; Joseph, E. A.; Kellock, A. J.; Arellano, N.; Kurdi, B. N.; Gopalakrishnan, K. In *Sub-30nm Scaling and High-Speed Operation of Fully-Confined Access-Devices for 3d Crosspoint Memory Based on Mixed-Ionic-Electronic-Conduction (Miec) Materials*; 2012 International Electron Devices Meeting, 10−13 Dec 2012; 2012; pp 2.7.1−2.7.4.
(18) Anbarasu, M.; Wimmer, M.; Bruns, G.; Salinga, M.; Wuttig, M. Nanosecond Threshold Switching of $GeTe_6$ Cells and Their Potential as Selector Devices. *Appl. Phys. Lett.* **2012**, *100* (14), 143505.
(19) DerChang, K.; Tang, S.; Karpov, I. V.; Dodge, R.; Klehn, B.; Kalb, J. A.; Strand, J.; Diaz, A.; Leung, N.; Wu, J.; Sean, L.; Langtry, T.; Kuo-wei, C.; Papagianni, C.; Jinwook, L.; Hirst, J.; Erra, S.; Flores, E.; Righos, N.; Castro, H.; Spadini, G. In *A Stackable Cross Point Phase Change Memory*, 2009 IEEE International Electron Devices Meeting (IEDM): 7−9 Dec 2009; 2009; pp 1−4.
(20) Lee, M.; Lee, D.; Kim, H.; Choi, H.; Park, J.; Kim, H. G.; Cha, Y.; Chung, U.; Yoo, I.; Kim, K. In *Highly-Scalable Threshold Switching Select Device Based on Chalcogenide Glasses for 3D Nanoscaled Memory Arrays*; 2012 International Electron Devices Meeting, 10−13 Dec 2012; 2012; pp 2.6.1−2.6.3.
(21) Kim, S.; Liu, X.; Park, J.; Jung, S.; Lee, W.; Woo, J.; Shin, J.; Choi, G.; Cho, C.; Park, S.; Lee, D.; Cha, E.; Lee, B.; Lee, H. D.; Kim, S. G.; Chung, S.; Hwang, H. In *Ultrathin (<10nm) Nb_2O_5/NbO_2 Hybrid Memory with Both Memory and Selector Characteristics for High Density 3D Vertically Stackable RRAM Applications*; 2012 Symposium on VLSI Technology (VLSIT), 12−14 June 2012; 2012; pp 155−156.
(22) Liu, X.; Sadaf, S. M.; Son, M.; Shin, J.; Park, J.; Lee, J.; Park, S.; Hwang, H. Diode-Less Bilayer Oxide (WO_x−NbO_x) Device for Cross-Point Resistive Memory Applications. *Nanotechnology* **2011**, *22* (47), 475702.
(23) Son, M.; Lee, J.; Park, J.; Shin, J.; Choi, G.; Jung, S.; Lee, W.; Kim, S.; Park, S.; Hwang, H. Excellent Selector Characteristics of Nanoscale VO_2 for High-Density Bipolar ReRAM Applications. *IEEE Electron Device Lett.* **2011**, *32* (11), 1579−1581.
(24) Son, M.; Liu, X.; Sadaf, S. M.; Lee, D.; Park, S.; Lee, W.; Kim, S.; Park, J.; Shin, J.; Jung, S.; Ham, M.; Hwang, H. Self-Selective Characteristics of Nanoscale VO Devices for High-Density ReRAM Applications. *IEEE Electron Device Lett.* **2012**, *33* (5), 718−720.
(25) Bricalli, A.; Ambrosi, E.; Laudato, M.; Maestro, M.; Rodriguez, R.; Ielmini, D. In *SiO_x-Based Resistive Switching Memory (RRAM) for Crossbar Storage/Select Elements with High On/Off Ratio*; 2016 IEEE International Electron Devices Meeting (IEDM): 3−7 Dec 2016; 2016; pp 4.3.1−4.3.4.
(26) Hsiung, C.-P.; Liao, H.-W.; Gan, J.-Y.; Wu, T.-B.; Hwang, J.-C.; Chen, F.; Tsai, M.-J. Formation and Instability of Silver Nanofilament in Ag-Based Programmable Metallization Cells. *ACS Nano* **2010**, *4* (9), 5414−5420.
(27) Jiang, H.; Belkin, D.; Savel'ev, S. E.; Lin, S.; Wang, Z.; Li, Y.; Joshi, S.; Midya, R.; Li, C.; Rao, M.; Barnell, M.; Wu, Q.; Yang, J. J.; Xia, Q. A Novel True Random Number Generator Based on A Stochastic Diffusive Memristor. *Nat. Commun.* **2017**, *8* (1), 882.
(28) La Barbera, S.; Vuillaume, D.; Alibart, F. Filamentary Switching: Synaptic Plasticity through Device Volatility. *ACS Nano* **2015**, *9* (1), 941−949.
(29) Ohno, T.; Hasegawa, T.; Tsuruoka, T.; Terabe, K.; Gimzewski, J. K.; Aono, M. Short-Term Plasticity and Long-Term Potentiation Mimicked in Single Inorganic Synapses. *Nat. Mater.* **2011**, *10*, 591.
(30) Shukla, N.; Grisafe, B.; Ghosh, R. K.; Jao, N.; Aziz, A.; Frougier, J.; Jerry, M.; Sonde, S.; Rouvimov, S.; Orlova, T.; Gupta, S.; Datta, S. In *Ag/HfO_2 Based Threshold Switch with Extreme Non-Linearity for Unipolar Cross-Point Memory and Steep-Slope Phase-FETs*; 2016 IEEE International Electron Devices Meeting (IEDM): 3−7 Dec 2016; 2016; pp 34.6.1−34.6.4.
(31) Song, J.; Park, J.; Moon, K.; Woo, J.; Lim, S.; Yoo, J.; Lee, D.; Hwang, H. In *Monolithic Integration of AgTe/TiO_2 Based Threshold Switching Device with TiN Liner for Steep Slope Field-Effect Transistors*; 2016 IEEE International Electron Devices Meeting (IEDM): 3−7 Dec 2016; 2016; pp 25.3.1−25.3.4.
(32) Song, J.; Prakash, A.; Lee, D.; Woo, J.; Cha, E.; Lee, S.; Hwang, H. Bidirectional Threshold Switching in Engineered Multilayer (Cu_2O/Ag:Cu_2O/Cu_2O) Stack for Cross-Point Selector Application. *Appl. Phys. Lett.* **2015**, *107* (11), 113504.
(33) Song, J.; Woo, J.; Lee, S.; Prakash, A.; Yoo, J.; Moon, K.; Hwang, H. Steep Slope Field-Effect Transistors With Ag/TiO_2-Based Threshold Switching Device. *IEEE Electron Device Lett.* **2016**, *37* (7), 932−934.
(34) Song, J.; Woo, J.; Prakash, A.; Lee, D.; Hwang, H. Threshold Selector with High Selectivity and Steep Slope for Cross-Point Memory Array. *IEEE Electron Device Lett.* **2015**, *36* (7), 681−683.
(35) Sun, H.; Liu, Q.; Li, C.; Long, S.; Lv, H.; Bi, C.; Huo, Z.; Li, L.; Liu, M. Direct Observation of Conversion Between Threshold Switching and Memory Switching Induced by Conductive Filament Morphology. *Adv. Funct. Mater.* **2014**, *24* (36), 5679−5686.
(36) van den Hurk, J.; Linn, E.; Zhang, H.; Waser, R.; Valov, I. Volatile Resistance States in Electrochemical Metallization Cells Enabling Non-Destructive Readout of Complementary Resistive Switches. *Nanotechnology* **2014**, *25* (42), 425202.
(37) Wang, Z.; Joshi, S.; Savel'ev, S. E.; Jiang, H.; Midya, R.; Lin, P.; Hu, M.; Ge, N.; Strachan, J. P.; Li, Z.; Wu, Q.; Barnell, M.; Li, G.-L.; Xin, H. L.; Williams, R. S.; Xia, Q.; Yang, J. J. Memristors with Diffusive Dynamics as Synaptic Emulators for Neuromorphic Computing. *Nat. Mater.* **2017**, *16*, 101.
(38) Yoo, J.; Woo, J.; Song, J.; Hwang, H. Threshold Switching Behavior of Ag-Si Based Selector Device and Hydrogen Doping Effect on Its Characteristics. *AIP Adv.* **2015**, *5* (12), 127221.
(39) Yu, M.; Fang, Y.; Wang, Z.; Pan, Y.; Li, M.; Cai, Y.; Huang, R. Self-Selection Effects and Modulation of TaO_x Resistive Switching Random Access Memory with Bottom Electrode of Highly Doped Si. *J. Appl. Phys.* **2016**, *119* (19), 195302.
(40) Zhao, X.; Xu, H.; Wang, Z.; Zhang, L.; Ma, J.; Liu, Y. Nonvolatile/Volatile Behaviors and Quantized Conductance Observed in Resistive Switching Memory Based on Amorphous Carbon. *Carbon* **2015**, *91*, 38−44.

DOI: 10.1021/acsaelm.9b00446
ACS Appl. Electron. Mater. 2019, 1, 2076−2085

(41) Chen, W.; Barnaby, H. J.; Kozicki, M. N. Volatile and Non-Volatile Switching in Cu-SiO_2 Programmable Metallization Cells. *IEEE Electron Device Lett.* **2016**, *37* (5), 580−583.
(42) Lim, S.; Yoo, J.; Song, J.; Woo, J.; Park, J.; Hwang, H. In *Excellent Threshold Switching Device (I_{off} ∼ 1 pA) with Atom-Scale Metal Filament for Steep Slope (< 5 mV/Dec), Ultra Low Voltage (V_{dd} = 0.25 V) FET Applications*; 2016 IEEE International Electron Devices Meeting (IEDM): 3−7 Dec 2016; 2016; pp 34.7.1−37.7.4.
(43) Liu, T.; Verma, M.; Kang, Y.; Orlowski, M. Volatile Resistive Switching in Cu/TaO_x/δ-Cu/Pt Devices. *Appl. Phys. Lett.* **2012**, *101* (7), 073510.
(44) Luo, Q.; Xu, X.; Liu, H.; Lv, H.; Gong, T.; Long, S.; Liu, Q.; Sun, H.; Banerjee, W.; Li, L.; Lu, N.; Liu, M. In *Cu BEOL Compatible Selector with High Selectivity (>10^7), Extremely Low Off-Current (∼pA) and High Endurance (>10^{10})*, 2015 IEEE International Electron Devices Meeting (IEDM): 7−9 Dec 2015; 2015; pp 10.4.1−10.4.4.
(45) Woo, J.; Lee, D.; Cha, E.; Lee, S.; Park, S.; Hwang, H. Control of Cu Conductive Filament in Complementary Atom Switch for Cross-Point Selector Device Application. *IEEE Electron Device Lett.* **2014**, *35* (1), 60−62.
(46) Liu, Q.; Sun, J.; Lv, H.; Long, S.; Yin, K.; Wan, N.; Li, Y.; Sun, L.; Liu, M. Real-Time Observation on Dynamic Growth/Dissolution of Conductive Filaments in Oxide-Electrolyte-Based ReRAM. *Adv. Mater.* **2012**, *24* (14), 1844−1849.
(47) Hubbard, W. A.; Kerelsky, A.; Jasmin, G.; White, E. R.; Lodico, J.; Mecklenburg, M.; Regan, B. C. Nanofilament Formation and Regeneration During Cu/Al_2O_3 Resistive Memory Switching. *Nano Lett.* **2015**, *15* (6), 3983−3987.
(48) Wang, Z.; Rao, M.; Midya, R.; Joshi, S.; Jiang, H.; Lin, P.; Song, W.; Asapu, S.; Zhuo, Y.; Li, C.; Wu, H.; Xia, Q.; Yang, J. J. Threshold Switching of Ag or Cu in Dielectrics: Materials, Mechanism, and Applications. *Adv. Funct. Mater.* **2018**, *28* (6), 1704862.
(49) Du, G.; Wang, C.; Li, H.; Mao, Q.; Ji, Z. Bidirectional threshold switching characteristics in Ag/ZrO2/Pt electrochemical metallization cells. *AIP Adv.* **2016**, *6* (8), 085316.
(50) Yang, Y.; Gao, P.; Gaba, S.; Chang, T.; Pan, X.; Lu, W. Observation of conducting filament growth in nanoscale resistive memories. *Nat. Commun.* **2012**, *3*, 732.
(51) Karpov, V. G.; Kryukov, Y. A.; Savransky, S. D.; Karpov, I. V. Nucleation switching in phase change memory. *Appl. Phys. Lett.* **2007**, *90* (12), 123504.
(52) Nardone, M.; Karpov, V. G.; Jackson, D. C. S.; Karpov, I. V. A unified model of nucleation switching. *Appl. Phys. Lett.* **2009**, *94* (10), 103509.
(53) Pevtsov, A. B.; Medvedev, A. V.; Kurdyukov, D. A.; Il'inskaya, N. D.; Golubev, V. G.; Karpov, V. G. Evidence of Field-Induced Nucleation Switching in Opal: Vo_2 Composites And Vo_2 Films. *Phys. Rev. B: Condens. Matter Mater. Phys.* **2012**, *85* (2), 024110.
(54) Chai, Z.; Ma, J.; Zhang, W.; Govoreanu, B.; Simoen, E.; Zhang, J. F.; Ji, Z.; Gao, R.; Groeseneken, G.; Jurczak, M. In *RTN-Based Defect Tracking Technique: Experimentally Probing The Spatial and Energy Profile of The Critical Filament Region and Its Correlation with HfO_2 RRAM Switching Operation and Failure Mechanism*, 2016 IEEE Symposium on VLSI Technology: 14−16 June 2016; 2016; pp 1−2.
(55) Soni, R.; Meuffels, P.; Petraru, A.; Weides, M.; Kügeler, C.; Waser, R.; Kohlstedt, H. Probing Cu Doped $Ge_{0.3}se_{0.7}$ Based Resistance Switching Memory Devices with Random Telegraph Noise. *J. Appl. Phys.* **2010**, *107* (2), 024517.
(56) Chai, Z.; Zhang, W.; Degraeve, R.; Zhang, J. F.; Marsland, J.; Fantini, A.; Garbin, D.; Clima, S.; Goux, L.; Kar, G. S. RTN in Ge_xse_{1-X} Ots Selector Devices. *Microelectron. Eng.* **2019**, *215*, 110990.

DOI: 10.1021/acsaelm.9b00446
ACS Appl. Electron. Mater. 2019, 1, 2076−2085